MR-Elastography

Ralph Sinkus, PhD
Ecole Supérieure de Physique et de Chimie Industrielles de la Ville de Paris

Introduction

Palpation has ever since been an important part of diagnostic procedures. This holds in case of breast cancer diagnosis, prostate cancer diagnosis as well as for instance for the assessment of liver fibrosis [1]. Thus, it is well known that pathological changes lead to alternations in the viscoelastic properties of tissue. As such, the assessment of viscoelastic properties might provide additional information useful for clinical diagnosis. Unfortunately, none of the commonly used non-invasive imaging techniques (ultrasound, CT and MRI) are directly sensitive to the physical parameters elasticity or viscosity. Therefore, those properties can only be obtained indirectly. There is actually a close physical link between the propagation of acoustic waves in a viscoelastic medium and its viscoelastic properties. Thus, the concept of elastography is

- to somehow generate acoustic waves within the medium,
- to measure those waves via a non-invasive imaging technique, and finally
- reconstruct maps of the viscoelastic properties from the measured wave fields.

The last step, i.e. converting the measured wave fields into maps of elasticity and viscosity, necessitates utilization of rheology, i.e. the theory explaining the relationship between stress and strain [2]. As will be explain later, it is not evident which rheological model is applicable for tissue (especially for tumors). Thus, quoting values for viscoelastic properties always depends upon the model used for interpreting the raw data.

The roots of elastography can be found in ultrasound, where 1D speckle cross-correlation was proposed to track tissue motion [3]. Thereby, the strain response caused by an externally applied stress is assessed. The field of ultrasound elastography has vastly evolved ever since. However, many applications are still confined to 1D. Here, MRI offers the unique opportunity to measure without any difficulties the 3D wave field within a volume and hence enabling an unbiased reconstruction. For the first time it was Lewa [4] who proposed to use MRI for measuring the displacement field caused by an acoustic wave and hence assessing viscoelastic properties of tissue. This idea was further developed by Muthupillai [5] and then picked up by the MR-community [6-9].

As mentioned before, elastography is basically an acoustic experiment with the MRI/ultrasound serving as an expensive/cheap camera whose sole purpose is to measure the generated wave field. The finger-prints of the true underlying rheology of the tissue are unfortunately hidden in the parameters associated with the propagation of the acoustic wave. Thus, full insight into the viscoelastic nature of the material can only be obtained by measurements at various frequencies. Hence, elastography for different frequency domains has been developed:

1. the quasi-static limit for $\nu \rightarrow 0$ [7],
2. the dynamic mono-chromatic case with $\nu=\nu_0 \in$ [50-500] Hz [8,10,11] and
3. the transient broadband case [12,13].

In case of linear isotropic viscoelasticity, there is at each frequency only one complex number describing the properties of the relatively slow shear wave (which is the source of the contrast in elastography as explained later), i.e. the complex shear modulus $G(\omega)=G_d(\omega)+iG_l(\omega)$ with G_d the dynamic modulus and G_l the loss modulus. Typical dispersion curves for both moduli are sketched in Fig.1 for a viscoelastic tissue-like solid with three regimes to be analyzed:

I. the dynamic modulus approaches in the low-frequency limit the so-called rubbery plateau with $G_d \rightarrow \mu_0$=constant and $G_l \rightarrow 0$,
II. at intermediate frequencies the two curves are close to each other with similar slopes $\sim\omega^{\alpha}$ (α~0.75 for the cytoplasma [14] and α~0.15 for the cytoskeleton [15]), and
III. at high frequencies the smallest viscoelastic structures are ultimately probed which leads for the dynamic modulus to the so-called glassy region, i.e. $G_d \rightarrow \mu_\infty$ [16]. The fate of the loss modulus depends strongly upon the rheology of the material, it can either further rise or drop.

When performing a non-static ($\nu>0$) elastography experiment, it is a priori not known which frequency regime is applicable (II or III) because their onsets depend upon intrinsic relaxation times (which have to be measured). The strong impact of the chosen rheological model for interpreting G_d and G_l in terms of elasticity and viscosity on the diagnostic value of the data will be shown later in case of breast tumor data. In that sense MR-elastography might serve as a tool to understand the rheology of pathologies. It carries the potential to add valuable information to the diagnostic chain but should not be considered as a stand-alone modality for breast cancer detection [1]: for instance, it is well known that lobular invasive carcinoma are sometimes non-palpable (probably due to missing stroma reaction) and that benign fibrocystic alterations of

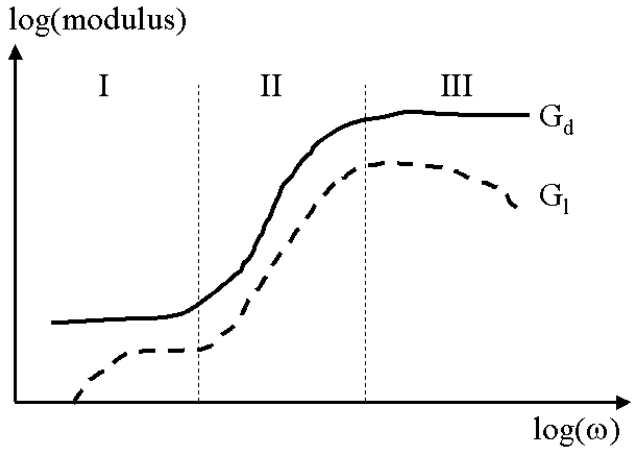

Fig.1: Sketch of the typical dispersion properties of a viscoelastic solid. At low frequencies the rubbery plateau dominates, i.e. $G_d=\mu_0$=constant and $G_l \rightarrow 0$. At intermediate frequencies both rise according to a power-law in tissue. The high-frequency limit is denoted as the glassy region where $G_d=\mu_\infty$ is again constant.

breast tissue (mastopathy) can often be very well palpable. Thus, it is reasonable to view the viscoelastic parameters in combination with already established diagnostic information, for instance the enhancement characteristics of a contrast agent bolus. In case of liver fibrosis, on the other hand, elastography might provide significant help to evaluate the efficacy of antiviral/antifibrotic treatments [17,18].

Theory of Shear Wave Propagation and Rheology

Two kinds of waves are generated when pushing on a viscoelastic medium: compressional waves and transversal waves. In tissue, which is quasi-incompressible, this leads to an enormous imbalance between the speeds of the individual waves: the compressional wave travels at about 1550 m/s while the transversal (or shear) wave travels at 1-10 m/s. This difference in order of magnitude is found back in the according material parameters, i.e. the 2nd Lamé coefficient λ (describing the effect of compression) and the shear modulus μ (handling the effect of shearing the material) differ by 6 orders of magnitude! The corresponding equation of motion is

$$\rho \partial_t^2 \vec{u}(\vec{x},t) = \mu \nabla^2 \vec{u}(\vec{x},t) + (\lambda+\mu)\nabla(\nabla \vec{u}(\vec{x},t)) \qquad , \tag{1}$$

with ρ the density of the material and $\vec{u}(\vec{x},t)$ the displacement vector at position $\vec{x}$ and time t (assuming local homogeneity). Due to the almost incompressible nature of tissue the value of $\nabla \vec{u}(\vec{x},t)$ is so small that it is not feasible to evaluate this term given normal values of SNR (~10%) and finite spatial resolution (~1-2mm). The small magnitude of this term is minutely balanced by the large magnitude of the 2nd Lamé coefficient λ [11]. Thus, it is meaningful to rewrite Eq.1 by introducing the pressure $p = (\lambda+\mu)\nabla \vec{u}(\vec{x},t)$, i.e.

$$\rho \partial_t^2 \vec{u}(\vec{x},t) = \mu \nabla^2 \vec{u}(\vec{x},t) + \nabla p \qquad , \tag{2}$$

which resembles Eq.1 in case of local homogeneity. Otherwise, it is the correct extension for the pressure term in case of local heterogeneity. The pressure p represents the part originating from the compressional wave field and must not be neglected. Since elastography operates in the near field of the vibrational source, it is not evident that the contributions of the term ∇p can simply be eliminated by low-pass filters, which is motivated by the large wavelength of the compressional wave. An unbiased method is the application of the curl-operator because the rotation of the gradient of a scalar field is identical to zero (certainly introducing more noise due to the application of an additional derivative). This yields a Helmholz equation which simplifies in case of mono-chromatic excitation (i.e. $\vec{u}(\vec{x},t) = \vec{u}(\vec{x})\exp(i\omega t)$) to

$$-\rho\omega^2 \vec{q}(\vec{x}) = G^*(\omega)\nabla^2 \vec{q}(\vec{x}) \qquad , \qquad \vec{q}(\vec{x}) = \nabla \times \vec{u}(\vec{x}) \in \mathbb{C}^3 \qquad . \tag{3}$$

Here, the shear modulus $G^*(\omega) = G_d(\omega) + iG_l(\omega)$ is introduced whose complex-valued extension shall account for loss effects. This ad-hoc method of introducing viscose effects can certainly not resemble true nature and it is now necessary to link G_d and G_l to a particular rheological model in order to interpret these values in terms of spring constants μ and dashpot constants η. It is important to realize, that Eq.3 provides at most one complex number (i.e. $G^*(\omega)$) although there are three equations! This is due to the assumption of isotropy. It is certainly feasible to go beyond isotropy and assume for instance locally a transverse

anisotropic material [19,20]. This complicates the equations significantly but does not resolve the difficulty to interpret the data by a rheological model.

Fig.2 shows three common rheological models, i.e. a) the Voigt model with spring and dashpot in parallel, b) the Maxwell model with spring and dashpot in series and finally c) the more advanced springpot model, which resembles a fractal arrangement of an infinite series of Maxwell units. The link between rheological model and complex shear modulus is rather simple in case of the Voigt model:

$$G_d = \mu \quad , \quad G_l = \omega\eta \qquad . \tag{4}$$

The causality principle (Kramers-Kronig relations [21,22]) enforces actually a relationship between the dynamic and the loss modulus, which is suppressed in this particular model due to the specific exponent of the power-law (α=1) for the loss modulus. However, a constant value for G_d as well as G_l rising with $\sim\omega^1$ as a function of frequency is not what is observed in tissue [23,24] neither what has been measured on the cellular level [25]. The Maxwell model provides a frequency dependent complex modulus with

$$G_d = \frac{\mu}{1+\left(\frac{\mu}{\omega\eta}\right)^2} \quad , \quad G_l = \frac{\omega\eta}{1+\left(\frac{\omega\eta}{\mu}\right)^2} \tag{5}$$

and exhibits a high frequency limit, i.e. a glassy plateau. A low frequency limit could easily be generated by adding a spring in parallel to the dashpot leading to the Zener model. None of the classical models with a finite number of springs and dashpots is capable to generate a power-law behavior for G_d and G_l [26]. Such kind of property reflects a broad internal distribution of relaxation constants and is linked to so-called fractional derivatives [27]. It can be shown that an infinite series of Maxwell units – coupled in a fractal manner – provides a power-law. The exponent is linked to the degree of interconnection, i.e. α close to one indicates a loose coupling while α close to zero shows strong coupling [28]. In gelatin phantoms, typically, very low values are found which resembles their tight organization [29]. It is important to realize that it is not possible to distinguish properly between the different models when considering only the speed of the wave because the phase information within the complex shear modulus is ignored.

MR-Elastography Sequence

The concept of the MRE sequence is similar to the classical MR diffusion sequence. The different components of the mechanical wave can be measured in case of a mono-chromatic excitation using a modified spin-echo pulse-sequence (Fig. 3). A sinusoidal flow-encoding gradient (FEG) is placed prior and after the π-pulse with its shape equal to the pulse shape of the mechanical excitation [9]. The gradient channel to which the FEG is added determines which component of $\vec{u}(\vec{x},t)$ is measured. Thereby, the

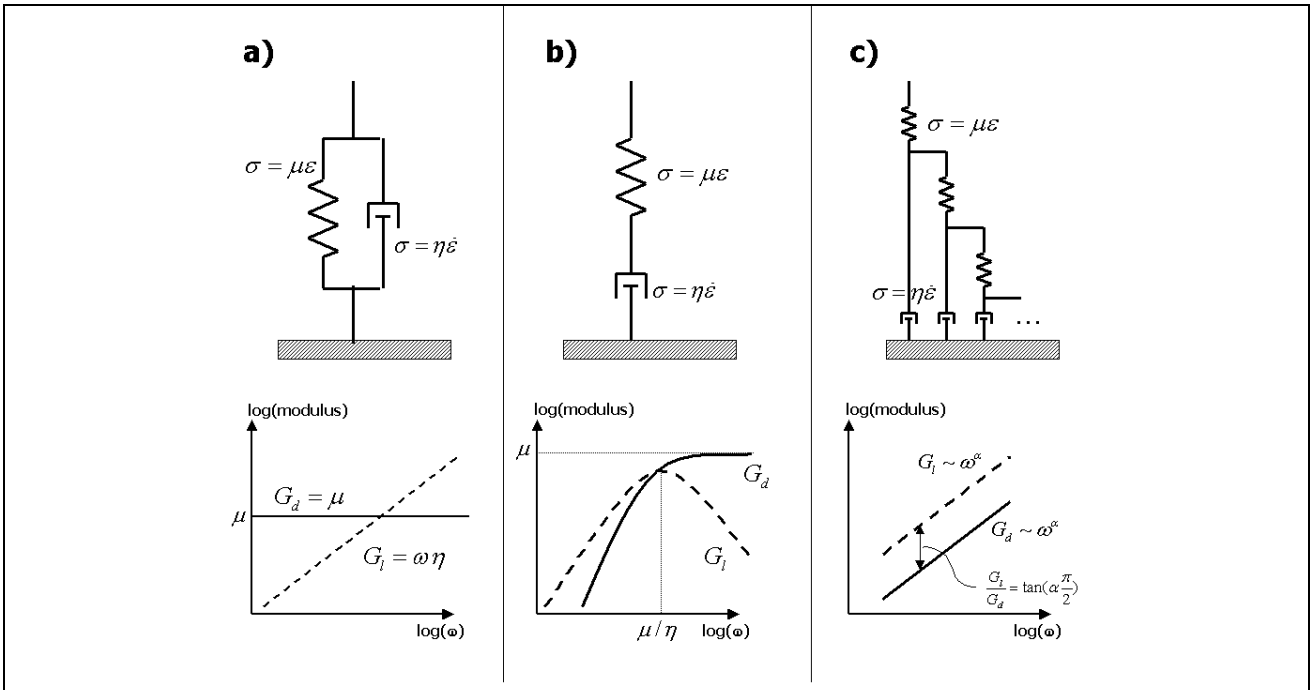

Fig.2: Three different rheological models: a) Voigt model with spring and dashpot in parallel. b) Maxwell model with spring and dashpot in series and c) springpot model with a fractal arrangement of Maxwell units.

phase of the final MR-image is directly proportional to the value of the corresponding wave-component at a given phase of the oscillatory cycle [30]. Possible wraps within the MR-phase-images obstruct this straightforward relationship and necessitate utilization of unwrapping algorithm. The repetition time TR is chosen such that the sequence is phase-locked to the mechanical excitation frequency ν, i.e., $TR = N \cdot T$, with $T = 1000/\nu\,[\mathrm{ms}]$ the basic interval and N an integer number. The same holds for the time separation between the beginning of the first FEG and the end of the last FEG, i.e., $TF = M \cdot T/2$ with M an integer number. An additional time delay TD allows to shift the phase between the onset of the mechanical excitation and the beginning of the imaging sequence. Thereby, snap-shots of the moving wave can be measured at different times during the oscillatory cycle.

Alternatively, motion-sensitized gradient echo sequences can be used. Usually, this necessitates to measure each displacement field twice (with reversed motion encoding gradients) and subtract the images afterwards. Thereby, systematic phase errors are eliminated and the sensitivity to small displacements is doubled [30]. Similar sequences are possible for the assessment of quasi-static motion in case of $\nu \to 0$ [6,7]. Recently, balanced steady-state free precession (b-SSFP) sequences have been proposed for mono-chromatic MRE in order to significantly accelerate data acquisition [31]. The sequence demonstrates very high sensitivity to small cyclic motion due to a subtle interplay between the dynamic equilibrium state to alternating spin de-phasing. However, the amplification factor depends upon T2, which makes a straightforward inversion of Eq.3 not possible. Thus, when utilizing such kind of sequence for a heterogeneous material, it is necessary to acquire a detailed T2 map.

Reconstruction of the Complex Shear Modulus

Several techniques for the calculation of $G^*(\omega)$ have been proposed within the cited elastography papers. In general, it is obvious from Eq.3 that finding $G^*(\omega)$ necessitates the assessment of $\vec{u}(\vec{x},t)$ at various times of the oscillatory cycle in order to calculate its real and imaginary part [19]. Then, Eq.3 can be rewritten to:

$$-\rho\,\omega^2(\vec{q}^{\,\Re} + i\vec{q}^{\,\Im}) = (G_d + iG_l)\nabla^2(\vec{q}^{\,\Re} + i\vec{q}^{\,\Im}) = \left(G_d\nabla^2\vec{q}^{\,\Re} - G_l\nabla^2\vec{q}^{\,\Im}\right) + i\left(G_d\nabla^2\vec{q}^{\,\Im} + G_l\nabla^2\vec{q}^{\,\Re}\right) \quad . \quad (6)$$

Consequently, a reconstruction algorithm ignoring the complex-valued nature of the displacement field is prone to be provide biased values for G_d and G_l. There are in general two different approaches to obtain local maps for the complex shear modulus:

- the direct approach, i.e. solving Eq.6 locally with more or less assumptions in order to simplify things [9,11,32], or
- the indirect approach [7,8,33], i.e. calculating the expected displacement field within a small ROI based upon an initial guess for the distribution of the viscoelastic parameters and updating the guess iteratively via χ^2-minimization between simulated and measured displacement data.

Both approaches have pros and cons: the direct method is certainly more sensitive to noise while the indirect is sensitive to boundary conditions. An additional challenge in case of an indirect method is the proper calculation of the $\nabla\vec{u}$-term in Eq.1. Its true value in tissue is so minute (due to its quasi incompressible nature) that an estimation of λ is easily off by several order of magnitude (λ should be of the order of GPa to yield the correct speed of sound in tissue of ~1550 m/s).

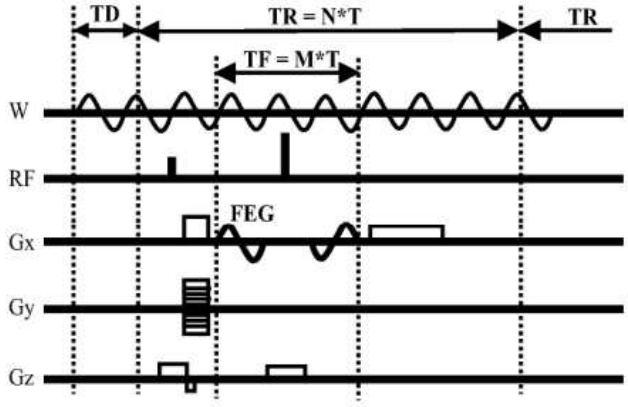

Fig.3: MR-sequence for the MRE experiment. A common spin-echo sequence is extended by sinusoidal flow-encoding gradients (FEG) located to both sides of the π-pulse. The timing of the sequence is tailored to be phase-locked to the mechanical stimulation (W).

It is important to realize that Eq.1 is local. Thus, reflections as well as mode conversion are properly taken into account as long as no additional simplifications are used. Otherwise, for instance evanescent waves generated at interfaces might easily obstruct the results. This leads actually to the issue of local homogeneity: Eq.1 is only valid if the spatial gradients of the viscoelastic parameters are locally negligible. Otherwise it is necessary to use the following equation

$$\rho \partial_t^2 u_i = \partial_{x_i}\left[\lambda \partial_{x_j} u_j\right] + \partial_{x_j}\left[\mu\left(\partial_{x_j} u_i + \partial_{x_i} u_j\right)\right] \quad , \qquad (7)$$

with $i \in [1,2,3]$ and Einstein convention for identical indices. This equation leads to a coupled system for all pixels within the region of interest and is thus rather challenging to solve. The assumption of local homogeneity (i.e. $\partial_{x_i}\mu = 0$) is certainly leading to artifacts at interfaces. In case of the direct approach the error stays however confined and does not propagate into other domains. The effect of ignoring the spatial derivatives of μ is identical to a reduction of the spatial resolution: a three-fold increase of the resolution would permit under the assumption of local homogeneity to calculate within each previous image-voxel all required derivatives.

Breast Cancer

Fig.4a) shows the experimental setup for in-vivo breast measurements. The patient is in prone position with the transducer attached from the side. This setting allows to first perform standard MR-mammography with contrast agent and apply afterwards MRE as an ad-on. A selected example for a palpable invasive ductal carcinoma is presented in Fig.4b). The subtraction image (with/without contrast agent) shows clearly the presence of a large strongly enhancing tumor. Fig.4c,d) are the corresponding images of the dynamic modulus and the loss modulus. Interestingly, the large tumor is barely visible in the map of G_d but well circumscribed in the image of G_l. When interpreting the data in terms of the Maxwell model, the tumor shows up extremely well in the shear modulus (Fig.4e). This example demonstrates, how significant the underlying rheology can change the diagnostic output. Fig.4f) resembles the current status of the clinical validation study performed at Tuebingen University [32]. Here, the shear modulus (Maxwell model) of 33 malignant tumors (red markers) und 18 benign lesions (green markers) is plotted versus the exponent of the power-law α ($\tan(\alpha\pi/2) = G_l / G_d$). Clearly, malignant lesions populate the high α – high $\mu^{Maxwell}$ region indicating a more loosely connected and hardened tissue architecture when compared to benign lesions.

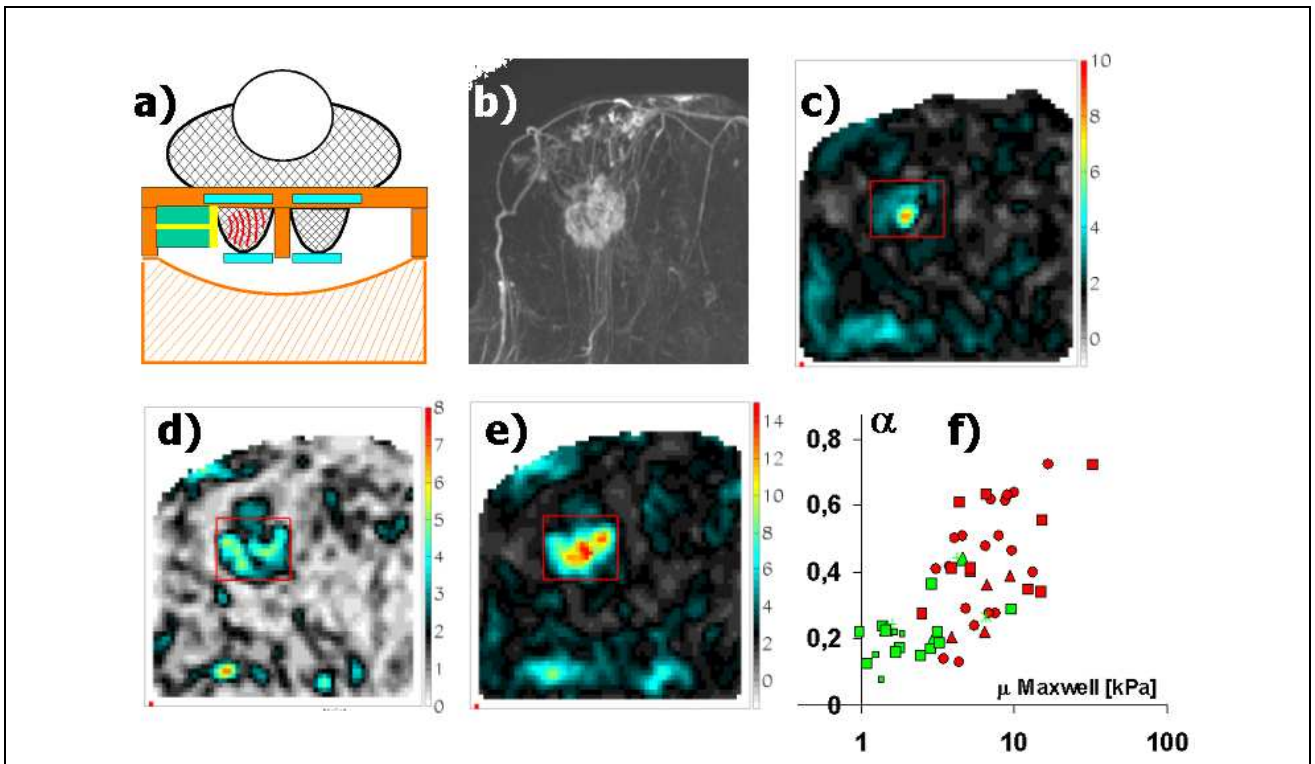

Fig.4: a) Schematic of the initial experimental setup. The transducer is attached from the side and generates longitudinal waves which traverse the breast. b) MR subtraction image in case of a ductal invasive carcinoma. c) Map of G_d [kPa] and d) map of G_l/ω [Pa*sec]. e) Map of $\mu^{Maxwell}$ [kPa] and f) compilation of clinical results obtained at Tuebingen University (α versus $\mu^{Maxwell}$).

Liver Fibrosis

Liver elastography has several challenges to overcome: firstly a mode of mechanical excitation such that the entire liver is properly illuminated by waves, and secondly potential respiratory motion if 3D displacement data are obtained within several slices. Efficient wave amplitude can be generated by exciting mainly compressional waves with the transducer. Those penetrate at low frequencies practically un-attenuated through the tissue and mode-convert at interfaces to shear waves. However, utilization of this method leads to a strong presence of the compressional wave in the data and thus necessitates the curl-operator for an unbiased reconstruction [11]. Respiration artifacts can be suppressed via utilization of navigators [35]. Fig. 5a,b) show the MR-magnitude image and the corresponding reconstructed map of G_d for a health volunteer. The liver appears rather homogeneous (as expected) with values around 2kPa. The kidney is anatomically well separated with an enhanced dynamic modulus. The correspondence to expected anatomy is extremely high demonstrating well that the suppression of motion artifacts has been successful. Mind, that the scan lasts over about 15mins depending on the efficiency of the navigator. A compilation of clinical results obtained at Hospital St. Luc is shown in Fig. 5c) [36]. Here, the shear modulus of the Maxwell model is plotted versus the degree of fibrosis of the liver (as established via biopsy). Clearly, elasticity is rising with increasing grade of fibrosis. Current work is dedicated to reduce scan time and improve data quality for an improved separation between the different grades of fibrosis.

Brain

Elastography of the brain was initially proposed in [37]. Here, a bite-bar is used to couple shear waves into the brain via the jaw [13]. The obtained values for the dynamic modulus still differ significantly among the different groups working on brain-MRE [13,38,39]. This is probably caused by two difficulties encountered in the brain: small vibrational amplitudes due to difficulties to efficiently generate shear waves inside the skull and strong viscosity of brain tissue [24] (see. Fig.6d). Latest results from the Prince of Wales Research Center [39] - taken at 90Hz mechanical excitation frequency - demonstrate a very high correspondence between maps of G_d and G_l and expected anatomy (Fig.6a-c). The ventricles are very well delineated from the white matter and exhibit strongly decreased values for both G_d and G_l. Since the ventricles represent cavities which contain the cerebrospinal fluid (CSF) it is reasonable that the shear properties drop because a perfect liquid cannot be sheared, i.e. $G_d=G_l=0$. Ex-vivo values for G_d and G_l found for porcine white matter via a classical vibrational rheometer (Fig.6d from [24]) actually agree very well with the values shown in Fig.6b,c). The small area below the ventricles exhibiting enhanced values for the dynamic modulus corresponds anatomically with the cingulate gyrus. Future work will be dedicated to patients suffering from hydrocephalus. Similar to what is observed in the ventricles, accumulation of serous fluid should significantly alter the viscoelastic properties.

Future

Elastography is an exciting area of current research. It combines MRI, propagation of acoustic waves in heterogeneous media, inversion techniques for partial differential equations and rheology. Elastography of the heart is certainly a challenging future topic. Apart from many different clinical applications, it is a unique tool to study the rheology of benign and malignant tissue in order to finally understand on a microscopic scale why we measure what we measure.

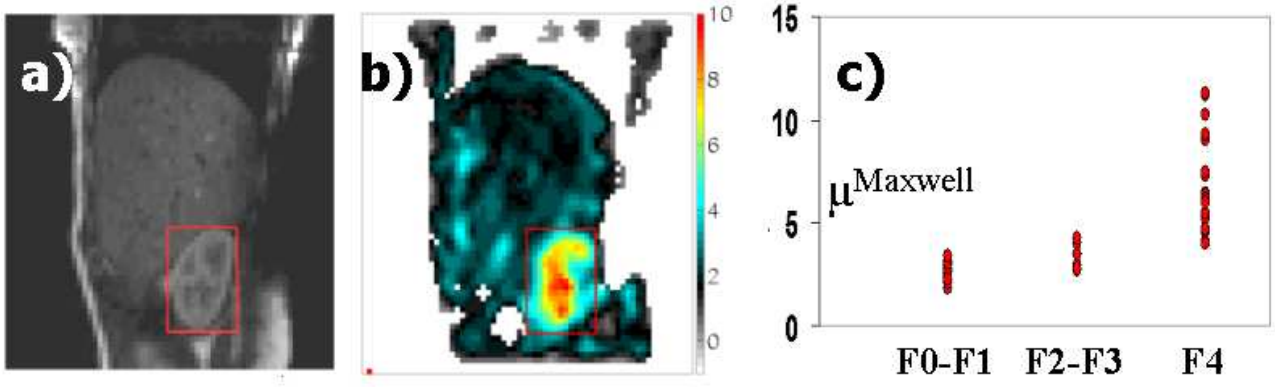

Fig.5: a) MR magnitude image of the liver (sagital orientation). The kidney is well visible (red rectangle). b) Corresponding map of G_d [kPa]. c) Compilation of clinical results obtained at Hospital St. Luc. Here, $\mu^{Maxwell}$ is plotted versus the fibrosis grade of the liver (values in units of kPa). Clearly, high grade fibrosis (F4) leads to an increased stiffness of the liver.

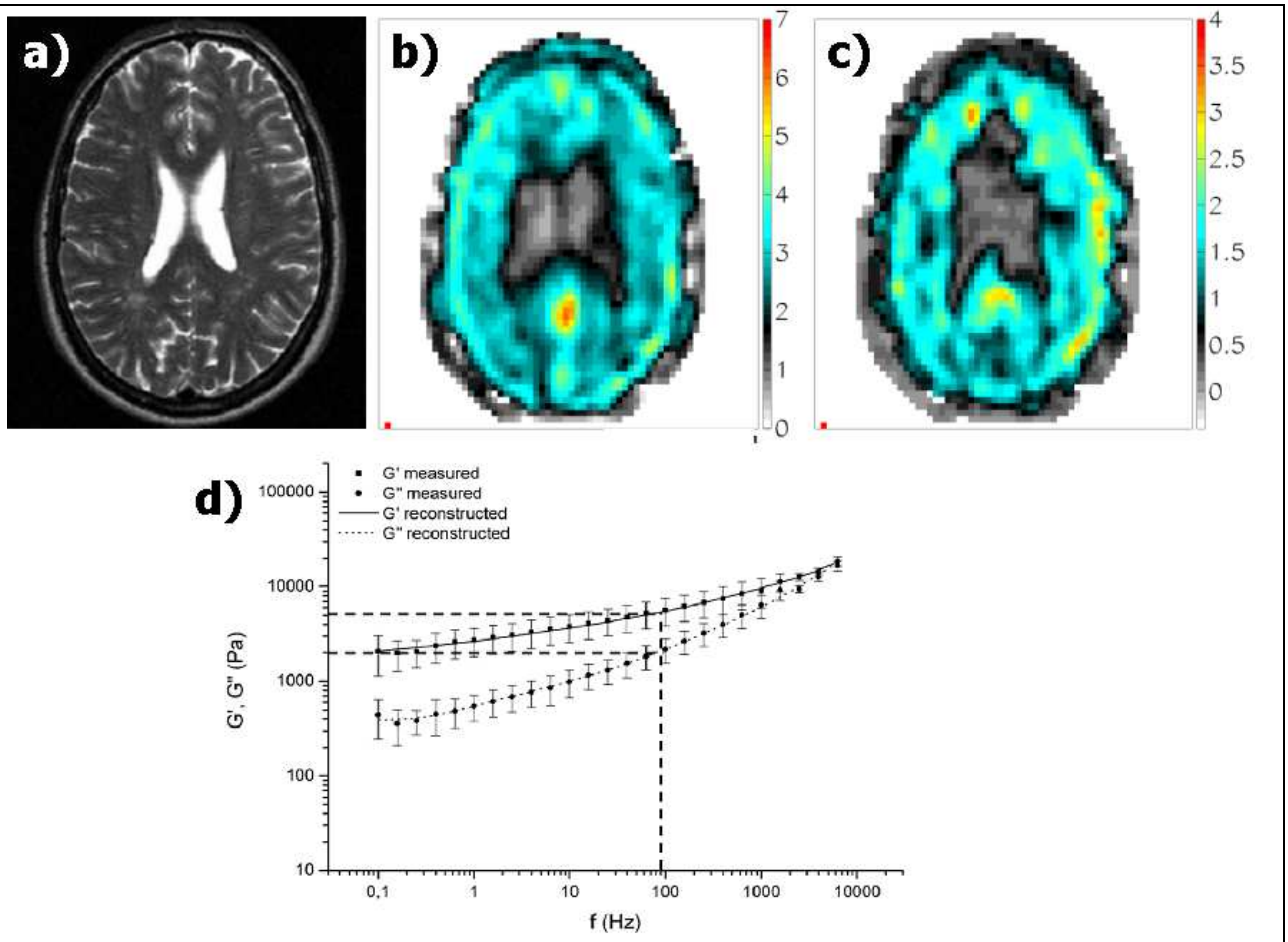

Fig.6: a) High resolution T2-weighted MR-magnitude image of the brain. The shown slice corresponds to the position of the obtained G_d (b) and G_l (c) maps (values in units of [kPa]). d) Dynamic shear moduli of the porcine white matter reconstructed from the relaxation spectrum and superimposed to measured data (from [24]).

Literature

[1] Nass SJ, Henderson IC, Lashof JC. Mammography and Beyond: Developing technologies for the early detection of breast cancer. National Academy Press, 2001.

[2] Verdier C, "Rheological Properties of Living Materials. From Cells to Tissues", Journal of Theoretical Medicine, June 2003, Vol. 5(2), pp. 67-91.

[3] Ophir J, Cespedes I, Ponnekanti H, Yazdi Y, Li X. "Elastography: a quantitative method for imaging the elasticity of biological tissues", Ultrason Imaging, vol. 13 (2), pp. 111-134, 1991.

[4] Lewa CJ, de Certaines JD. "MR imaging of viscoelastic properties", J Magn Reson Imaging. 1995 Mar-Apr;5(2):242-4.

[5] Muthupillai R, Lomas DJ, Rossman PJ, Greenleaf JF, Manduca A, Ehman RL. "Magnetic resonance elastography by direct visualization of propagating acoustic strain waves", Science. 1995 Sep 29;269(5232):1854-7.

[6] Plewes DB, Betty I, Urchuk SN, Soutar I. "Visualizing Tissue Compliance with MR Imaging", JMRI 5:733-738 (1995).

[7] Chenevert TL, Skovoroda AR, O'Donnel M, Emelianov SY. "Elasticity Reconstructive Imaging by Means of Stimulated Echo MRI", MRM 39: 482-490 (1998).

[8] Van Houten EE, Paulsen KD, Miga MI, Kennedy FE, Weaver JB. "An overlapping subzone technique for MR-based elastic property reconstruction", Magn Reson Med. 1999 Oct;42(4):779-86.

[9] Sinkus R, Lorenzen J, Schrader D, Lorenzen M, Dargatz M, Holz D. "High-resolution tensor MR elastography for breast tumour detection", Phys Med Biol. 2000 Jun;45(6):1649-64.

[10] Muthupilliai R, Rossman PJ, Lomas DJ, Greenleaf JF, Riederer SJ, Ehman RL. "Magnetic Resonance Imaging of Transverse Acoustic Strain Waves", MRM 36:266-274 (1996).

[11] Sinkus R, Tanter M, Xydeas T, Catheline S, Bercoff J, Fink M. "Viscoelastic shear properties of in vivo breast lesions measured by MR elastography", Magn Reson Imaging. 2005 Feb;23(2):159-65.

[12] Sandrin L, Tanter M, Catheline S, Fink M. “Shear Modulus Imaging using 2D transient elastography”, IEEE Trans. Ultrason., Ferroelec., Freq. Contr., vol. 49 (4), pp. 426-435, 2002.
[13] McCracken PJ, Manduca A, Felmlee J, Ehman RL. “Mechanical transient-based magnetic resonance elastography”, Magn Reson Med. 2005 Mar;53(3):628-39.
[14] Mason TG, Gisler T, Kroy K, Frey E, Weitz AD, “Rheology of F-actin solutions determined from thermally driven tracer motion”, J. Rheol. 44 (4), July/August 2000.
[15] Fabry B, Maksym GN, Butler JP, Glogauer M, Navajas D, Taback NA, Millet EJ, Fredberg JJ, “Time scale and other invariants of integrative mechanical behavior in living cells”, Physical Review E 68, 041914 (2003).
[16] Heymans N, “Constitutive equations for polymers viscoelasticity derived from hierarchical models in cases of failure of time-temperature superposition”, Signal Processing 83 (2003) 2345-2357.
[17] Peeters F, Sinkus R, Salameh N, Annet L, ter Beek LC, Van Beers BE, “In Vivo MR-Elastography of Liver Fibrosis”, Proc. Intl. Soc. Mag. Reson. Med. 13, p. 339 (2005).
[18] Rouviere O, Yin M, Dresner MA, Rossman PJ, Burgart LJ, Fidler JL, Ehman RL, “In Vivo MR Elastography of the Liver: Preliminary Results”, Proc. Intl. Soc. Mag. Reson. Med. 13, p. 340 (2005).
[19] Sinkus R, Tanter M, Catheline S, Lorenzen J, Kuhl C, Sondermann E, Fink M. “ Imaging anisotropic and viscous properties of breast tissue by magnetic resonance-elastography”, Magn Reson Med. 2005 Feb;53(2):372-87.
[20] Romano AJ, Abraham PB, Rossman PJ, Bucaro JA, Ehman RL. “Determination and analysis of guided wave propagation using magnetic resonance elastography”, Magn Reson Med. 2005 Oct;54(4):893-900.
[21] Kronig R de L. “On the theory of the dispersion of X-rays”, J. Opt. Soc. Am. 12, 547-557 (1926).
[22] Kramers HA. “La diffusion de la lumière par les atomes”, Atti. Congr. Intern. Fisica Como 2, 545-557 (1927).
[23] Kiss MZ, Varghese T, Hall TJ. “Viscoelastic characterization of in vitro canine tissue”, Phys. Med. Biol. 49 (2004) 4207-4218
[24] Nicolle S, Lounis M, Willinger R, Palierne JF. “Shear linear behavior of brain tissue over a large frequency range”, Biorheology 42 (2005) 209-223.
[25] Desprat N, Richert A, Simeon J, Asnacios A. “Creep function of a single living cell”, Biophys J. 2005 Mar;88(3):2224-33. Epub 2004 Dec 13.
[26] Schiessel H, Metzler R, Blumen A,Nonnenmacher TF, “Generalized viscoelastic models: their fractional equations with solutions”, J. Phys. A: Math. Gen. 28 (1995) 6567-6584.
[27] Bagley RL, “A Theoretical Basis for the Application of Fractional Calculus to Viscoelasticity”, J. Rheol. 27 (3), 201-210 (1983).
[28] Schiessel H, Blumen A, „Mesoscopic Pictures of Sol-Gel Transition: Ladder Models and Fractal Networks”, Macromolecules 1995, 28, 4013-4019.
[29] Chen Q, Suki B, An KN. „Dynamic Mechanical Properties of Agarose Gel by a Fractional Derivative Model“, 2003 Summer Bioengineering Conf. June 25-29, Florida.
[30] Muthupillai R, Rossmann PJ, Lomas DJ, Greenleaf JF, Riederer SJ, Ehman RL. “Magnetic Resonance Imaging of Transverse Acoustic Strain Waves”, MRM 26:266-274 (1996).
[31] Bieri O, Maderwald S, Ladd ME, Scheffler K. „Balanced Alternating Steady-State Elastography”, Proc. Intl. Soc. Mag. Reson. Med. 13, p 97 (2005).
[32] Oliphant TE, Manduca A, Ehman RL, Greenleaf JF. “Complex-valued stiffness reconstruction for magnetic resonance elastography by algebraic inversion of the differential equation”, Magn Reson Med. 2001 Feb;45(2):299-310.
[33] Van Houten EE, Miga MI, Weaver JB, Kennedy FE, Paulsen KD. “Three-dimensional subzone-based reconstruction algorithm for MR elastography”, Magn Reson Med. 2001 May;45(5):827-37.
[34] Xydeas T, Siegmann K, Sinkus R, Krainick-Strobel U, Miller S, Claussen CD. “ Magnetic resonance elastography of the breast: correlation of signal intensity data with viscoelastic properties”, Invest Radiol. 2005 Jul;40(7):412-20.
[35] Sinkus R, ter Beek LC, Peeters F, Annet L,Van Beers BE. “Navigator-Gated In-Vivo 3D Liver MR-Elastography”, Proc. Intl. Soc. Mag. Reson. Med. 13, p 624 (2005).
[36] Huwart L, Peeters P, Sinkus R, Annet L, Salameh N, ter Beek L, Horsmans Y, Van Beers BE. “Liver fibrosis: non-invasive assessment with three-dimensional MR elastography”, NMR in Biomedicine, submitted.
[37] Kruse SA, Dresner MA, Rossman PJ, Felmlee JP, Jack CR, Ehman RL. “Palpation of the brain using magnetic resonance elastography”, Proc. Int. Soc. Magn. Reson. Med. 7, 258 (1999).
[38] Uffmann K, Galban CJ, Maderwald S, Paul T, Schlamann MU, de Greiff A, Ladd ME. “MR Elastography of the Human Brain: Case Study Involving a Patient with a Temporal Glioma”, Proc. Intl. Soc. Mag. Reson. Med. 13, p 757 (2005).
[39] Green M, Sinkus R, Cheng S, Bilston L. ”3D MR-Elastography of the Brain at 3Tesla”, Proc. Intl. Soc. Mag. Reson. Med. 13, p 2176 (2005).